Topic area: **CMMSP**

Analysis of Intermetallic Phases in Aerospace Aluminium Alloys Using a Nuclear Microprobe and Phase Correlation Mapping

A.P. Boag[1*], D.G. McCulloch[1], D.N. Jamieson[2], S.M. Hearne[2], A.E. Hughes[3], C.G. Ryan[4], L.M. Pedrina[1] and B. Rout[2]

[1]*Applied Physics, School of Applied Science, RMIT University, GPO Box 2476V, Melbourne, VIC, 3001, Australia*
[2]*Microanalytical Research Centre, School of Physics, University of Melbourne, Victoria, 3010, Australia*
[3]*CSIRO, Division of Manufacturing and Infrastructure Technology, Private Bag 33 Clayton Sth MDC, Clayton, Vic, 3169, Australia*
[4]*CSIRO, Division of Exploration and Mining, Bayview Avenue, Clayton, VIC 3168, Australia*

e-mail of corresponding author: adam.boag@rmit.edu.au

Introduction

Aluminium alloys for commercial applications contain numerous intermetallic inclusions [1]. These inclusions typically take on many shapes and have diameters up to 50 μm on a rolled surface [2]. Particle surface densities ranging from 3 x 10^5 to 1 x 10^6 /cm^2 have been measured [2-4]. Exposed surfaces of these alloys require protection against corrosion. This is usually accomplished by means of a conversion coating using Cr compounds or anodising, followed by a paint system which may include a chromate inhibited primer and a topcoat. The breakdown of these coatings allows the onset of corrosion in the aluminium alloy which is a significant problem given the wide application of aluminium alloys in infrastructure and transport (particularly aerospace).

Pitting corrosion in aluminium alloys is particularly destructive since pitting can lead to other forms of corrosion such as exfoliation corrosion which undermines structural integrity [5]. Pitting corrosion is localised and it has been demonstrated that intermetallics play an important role in the formation of a pit [3,4]. The main focus of this paper is to determine whether a Nuclear Microprobe and Particle Induced X-ray Emission (PIXE) analysis combined with phase correlation mapping can be used to identify the different intermetallic phases present in the aerospace aluminium alloy AA2024-T3. This method can then be applied to investigate the association of particular intermetallics with the onset of deep pits in a corroded surface.

Experimental Method

The alloy samples

The Al-alloy AA2024-T3 [5] belongs to the 2XXX series of Al-Cu-Mg alloys and was the first of this type to have a yield strength approaching 490 MPa [5]. Its desirable properties include high strength and fatigue resistance [5]. It is used in aerospace applications like aircraft fuselage, wing skins and engine areas. The main alloying elements are Cu (3.8-4.9%) and Mg (1.2-1.8%). It also contains Si (0.5%), Fe (0.5%), Mn (0.3-0.9%), Cr (0.1%), Zn (0.25%) and Ti (0.15%). Polished substrates were prepared by pressing out discs of AA2024-

T3 sheet 1.6 mm thick. These discs were then ground using silicon carbide papers to P1200, before final polishing down with 0.25 µm diamond. Corrosion was initiated by placing the polished specimens in an aerated 0.1M NaCl solution, until corrosion in the form of pits was identified by hydrogen evolution at the surface.

Nuclear microprobe analysis

Samples were exposed to a 3.0 MeV proton beam. PIXE measurements were performed with an 80 µm thick Be filter (to reduce the aluminium signal). The Be filter was placed in front of the Ge X-ray detector located 165 mm from the sample stage. PIXE analysis and phase correlation mapping of the intermetallics and their individual elements were performed using GeoPIXE®.

Results for PIXE on standard alloys

In order to calibrate the phase correlation maps to reliably identify different intermetallic particles, four standard alloys were positioned in a checkerboard arrangement for PIXE analysis, see Figure 1. The chosen alloys represent the major classes of intermetallics in AA2024-T3: $CuAl_2$, $CuMgAl_2$, Cu_2FeAl_7 and $FeAl_3$ these are labelled 1-4 in the order listed. Although the samples are visible, it is difficult to distinguish the exact elemental compositions from these maps alone. For this reason, phase correlation diagrams were generated by selecting two aluminium elemental systems, and plotting the individual pixel intensities of the aluminium against the intensity of the element. The systems chosen were Al-Cu and Al-Fe shown in Figure 2 (a) and (b) respectively. As expected there are three clear phases present in the case of Al-Cu, arrows 1-3, while two phases are evident in the case of the Al-Fe, arrows 4-5.

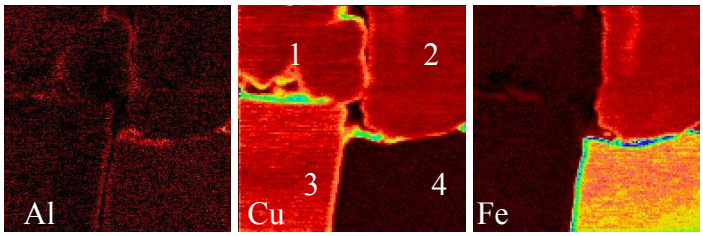

Figure 1: PIXE elemental maps for Al, Cu, Fe. Region 1-$CuMgAl_2$, 2.-Cu_2FeAl_7, 3-$CuAl_2$ and 4 -$FeAl_3$.

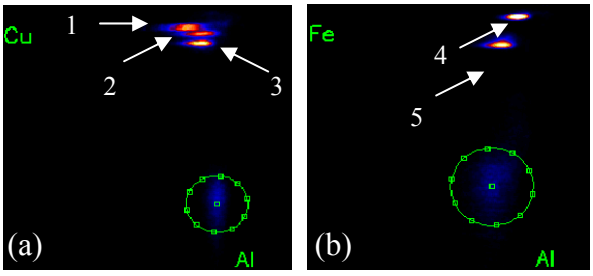

Figure 2: Phase correlation diagrams of the Al-elemental systems. (a) Al-Cu and (b) Al-Fe. Arrows 1-3 highlight the Al-Cu phases $CuAl_2$, $CuMgAl_2$ and $CuFeAl_7$, respectively. Arrows 4-5 represent the Al-Fe phases $FeAl_3$ and $CuFeAl_7$. The circled regions indicate noise.

The origin of the phase signals of the aluminium elemental systems were then physically correlated with the surface maps. Figure 3 shows these surface maps for aluminium elemental systems. The third system observed was the Cu_2FeAl_7 as aluminium is bonded to both copper and iron these maps were identical resulting in only four phase maps. On each map the aluminium elemental system observed is highlighted in green. Map 1 in Figure 3 shows the location of $CuAl_2$ on the surface; map 2 shows $CuMgAl_2$; map 3 Cu_2FeAl_7 and map 4 $FeAl_3$.

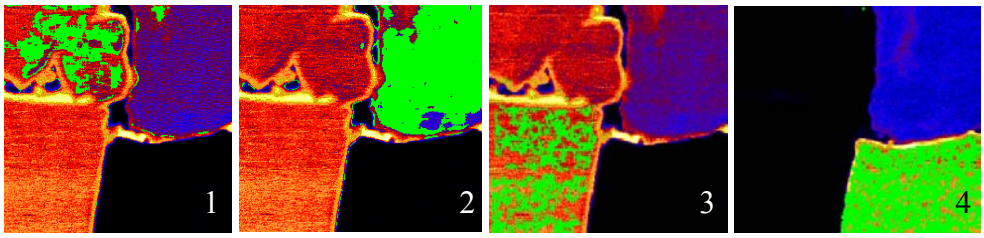

Figure 3: Origin of the phase signals of the four elemental systems; map 1 shows the location of $CuAl_2$; map 2 shows $CuMgAl_2$; map 3 Cu_2FeAl_7 and map 4 $FeAl_3$.

Results for PIXE on corroded AA2024-T3

This identification technique was then applied to AA2024-T3 alloy samples exposed to the NaCl solution. The analysis area was chosen to include two pits formed during exposure. Figure 4 shows Al, Cl, Cu, Mn and Fe PIXE elemental maps obtained. The circles indicate the location of the two corrosion pits, labelled 1 and 2 in Figure 4(a). Cl was concentrated in the centre of the pits, however at much lower concentrations in pit 2, see Figure 4(b). Cl has been found to be corrosive for aluminium and associated with pitting [3, 4, 7]. Pit 1 has a Cu-Mg-Al particle, also known as an S-phase particle next to the Cu-Mn-Fe-Al particle. This was identified by mapping the origin of phase signals back to the surface, this is discussed later, Figure 4(f) shows these particles in white and a large particle can be seen at Pit 1. Pit 2 has an Cu-Fe-Mn-Al inclusion this was also identified by phase mapping and is shown in black in Figure 4(f). A Cu rich region is shown as a higher intensity region to right hand side of pit 2 in Figure 4(c) and a white region in Figure 4(f). This may also be an S-phase particle. The coupling of these two types of intermetallic particles at a site of pit formation was evident in a number of maps taken of the corroded surface.

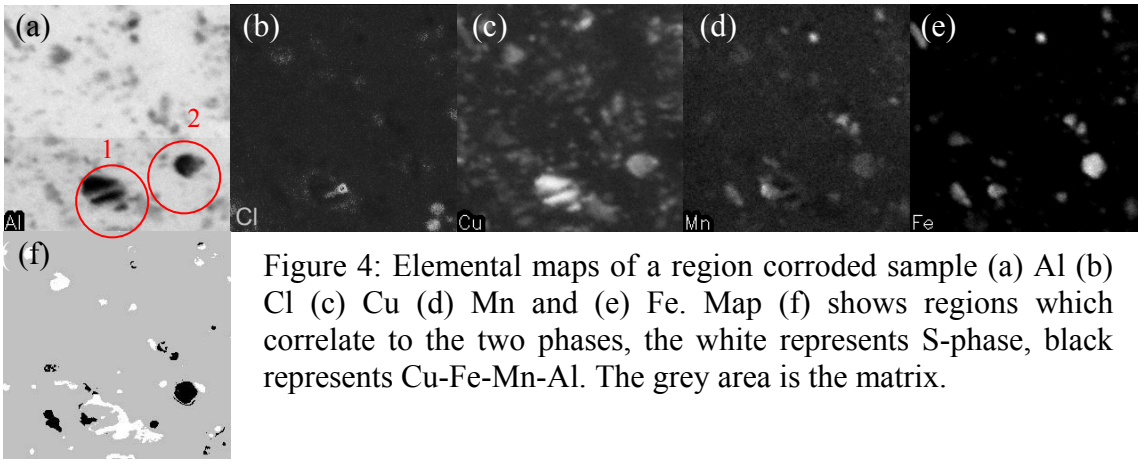

Figure 4: Elemental maps of a region corroded sample (a) Al (b) Cl (c) Cu (d) Mn and (e) Fe. Map (f) shows regions which correlate to the two phases, the white represents S-phase, black represents Cu-Fe-Mn-Al. The grey area is the matrix.

To investigate changes in the intermetallics phase maps for the corroded AA2024-T3 alloy sample were compared with phase maps of a polished AA2024-T3 reference sample. Areas on the phase correlation maps for the polished surface were highlighted and their relationship to areas on the elemental maps showed bright regions representing Cu in solid solution with the alloy. The presence of two main types of intermetallics is evident in the Al-Cu phase correlation map shown in Figure 5(a). The upper zone (arrow 1), has a higher Cu concentration, representing S-phase particles, the lower zone (arrow 2) represents Cu-Fe-Mn-Al particles.

By analysing the phase diagram for the corroding sample two major differences were observed. The first is that the S-phase zone extends to around ten times the Cu levels (with

decreasing Al levels) of the polished surface. The second difference is that the S-phase zone has split. See Figure 5(b) arrow 1. Both these changes are due to Cu-enrichment resulting from dealloying of the S-phase particles that lose Al ($Al \rightarrow Al^{3+} + 3e^-$) and Mg ($Mg \rightarrow Mg^{2+} + 2e^-$) producing a Cu residue [3,4]. There is also some evidence of Cu enrichment of the Cu-Mn-Fe-Al intermetallics indicated by the lengthening of the second phase shown in Figure 5(b) arrow 2. This could be due to the deposition of Cu from solution, since they are strong cathodes ($Cu^{2+} + 2e^- \rightarrow Cu$) observed by Wei et al. [4].

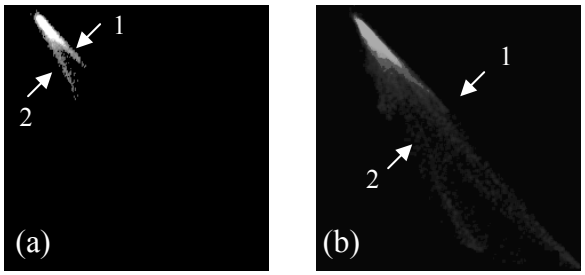

Figure 5: Al-Cu Phase correlation diagram for the (a) polished and (b) AA2024-T3 sample exposed to the NaCl solution. Arrow 1 represents S-phase particles and arrow 2 represents Cu-Fe-Mn-Al particles.

The S-phase and Cu-Mn-Fe-Al zones in Figure 5(b) were mapped back to the elemental maps to identify their locations, shown in Figure 4(f). The white regions represent the S-phase enrichment, the black regions represent the Cu-Mn-Fe-Al intermetallics and the grey area is the matrix. Both S-phase and Cu-Fe-Mn-Al particles were located around the pits. This shows that this pair of particles is associated with the establishment of pits. Pride et al. [7] have shown that pit formation only occurs when the current density to pit radius is greater than 2 mA/cm^2. High current densities could be established when the cathodic Cu-Fe-Mn-Al particles drive the dissolution of the anodic S-phase particles. While such dissolution would lead to Cu-enrichment it would also lead to a cavity in the surface where acidic conditions could be established and pitting could ensue.

Conclusion

This work shows that Nuclear Microprobe analysis combined with phase correlation mapping can be used to investigate rapidly the association between intermetallic particles and the site for corrosion pits in aluminium alloys. Paired S-phase and Cu-Fe-Mn-Al type intermetallic particles were found to be associated with pit sites in AA2024-T3 sample exposed to the NaCl solution.

Acknowledgements

The authors wish to thank Nigel Goodman for his role in the preparation of the samples.

References

[1] J.E. Hatch, American Society for Metals, Metals Park, OH, 1984 Chap pg
[2] L. Juffs, Masters Thesis, RMIT, 2002
[3] R. G. Buchheit, R. P. Grant, P. F. Hlava, B. Mckenzie And G. L. Zender: J. Electrochem. Soc., 1997, **144**, 2621-2628.
[4] G.S. Wei, M. Gao and R.P. Wei, Corrosion, January 1996, p. 8.
[5] Corrosion of Aluminium Alloys, ed J.R. Davis, ASM International (1999)
[6] S.T. Pride, J.R. Scully and J.L. Hudson, J. Electrochem. Soc., **141** (1994) 3028